# A constant self-consistent scattering lifetime in superconducting strontium ruthenate

Pedro L. Contreras E.

*Departamento de Física, Facultad de Ciencias, Universidad de Los Andes, Merida, 5101, Venezuela.*

Received 10 April 2024; accepted 10 June 2024

In this numerical work, we find a self-consistent constant scattering superconducting lifetime for two different values of the parameters, the inverse atomic strength, and the stoichiometric disorder in the triplet paired unconventional superconductor strontium ruthenate. This finding is relevant for experimentalists given that the expressions for the ultrasound attenuation and the electronic thermal conductivity depend on the superconducting scattering lifetime, and a constant lifetime fits well with non-equilibrium experimental data. Henceforth, this work helps experimentalists in their interpretation of the acquired data. Additionally, we encountered tiny imaginary parts of the self-energy that resemble the Miyake-Narikiyo tiny gap outside the unitary elastic scattering limit, and below the threshold zero gap value of 1.0 meV.

*Keywords:* Constant superconducting lifetime; strontium ruthenate; unconventional superconductivity; ultrasound attenuation; electronic thermal conductivity; self-consistent method.

DOI: https://doi.org/10.31349/RevMexFis.70.060501

## 1. Introduction

This study aims to understand how the scattering lifetime of the triplet-paired unconventional superconductor strontium ruthenate [1–6] is constant if calculated self-consistently in the presence of disorder. The existence of disorder in strontium ruthenate was proposed years ago [7]. A numerical answer appears by adding non-magnetic disorder and scanning the values of the zero superconducting gap $\Delta_0$, the inverse atomic strength $c$ and the stoichiometric disorder $\Gamma^+$ [8] using a self-consistent procedure. An elastic scattering lifetime is essential for non-equilibrium superconducting ultrasound attenuation and electronic thermal conductivity studies [9–14]. Therefore, we consider the self-consistent elastic cross-section to be a robust and powerful tool because it shows several hidden physical features. For example, tiny gaps or point nodes [15] due to the anisotropic parametrization with the same order parameter if it breaks the time-reversal symmetry as it happens in $Sr_2RuO_4$.

The original proposal of a constant superconducting lifetime in the non-equilibrium properties comes from the study [16]. Furthermore, experimental, theoretical, and numerical studies of the kinetic coefficient using the Green function formalism is a well-developed approach [9–14]. However, there was no understanding of why the superconducting lifetime has to be constant to fit experimental data in some alloys as outlined below with the respective references. Moreover, we understand from this work that the difficulty dwells in the self-consistent calculation of the imaginary cross-section term. This problem is related to the quantum mechanical non-relativistic scattering theory and the non-equilibrium statistical mechanics.

We mention three equations for the calculation of the scattering lifetime. First, for the distribution function $f_B(t)$ in the Boltzmann equation [17]. Second, if the quasi-classical probability density $W(t)$ is calculated using non-equilibrium statistical mechanics [18]. Third, for the characteristic time equation in a chemical reaction involving a reactant [A](t) [19]. In chemical kinetics, the self-consistent task is called the stiffness problem [19], which occurs when the dependent variable changes very fast. Table I summarizes the three non-equilibrium equations with a self-consistent lifetime problem. The solution is challenging for the first two beyond the $\tau$ approximation for electrons [20].

In this section, we briefly introduce a non-equilibrium property that fits well data if a constant scattering lifetime is used, that is, the superconducting ultrasound attenuation. An experimental ultrasound data in strontium ruthenate [21] was fitted successfully [22] using the directional superconducting ultrasound attenuation equation that comes from the Green function formalism

$$\frac{\alpha_j(T)}{\alpha_j(T_c)} = \frac{1}{2T}\frac{1}{\langle f_j^2\rangle}_{FS}\int_0^\infty d\epsilon\; A(\epsilon). \tag{1}$$

TABLE I. Kinetic equations with a self-consistent lifetime.

| Boltzmann equation for the distribution function $f(t)$ [17] | Probability density equation $W(t)$ [18] | Chemical reaction equation and its characteristic lifetime [19] |
|---|---|---|
| $(\frac{\partial f(t)}{\partial t})_{\text{coll}} + \frac{1}{\tau}\, f(t) = 0$ | $(\frac{\partial W(t)}{\partial t})_{\text{qsd}} + \frac{1}{\tau} W(t) = 0$ | $\frac{dA(t)}{\partial t} + \frac{1}{\tau} A(t) = 0$ |

In Eq. (1) the energy term is given by the expression

$$A(\epsilon) = \cosh^2\left(\frac{\epsilon}{2T}\right) \frac{\tau_s}{\tau_n} \frac{\langle f_j^2 \, \Re \, \sqrt{\epsilon^2 - \Delta_k^2}\rangle_{FS}}{\epsilon}. \quad (2)$$

The function $A(\epsilon)$ given by Eq. (2) shows the ratio of interest in this work explicitly ($\tau_s/\tau_n$). Equation (1) contains two terms averaged over the Fermi surface: First, the square of the electron-phonon matrix elements $f_j$, for the three elastic modes $j = P, T_1$, and $T_2$. Second, the real part of the root $\langle f_j^2 \, \Re \, \sqrt{\epsilon^2 - \Delta_k^2}\rangle_{FS}$ times the square of $f_j$. In addition, Eq. (2) has the trigonometric factor that is the negative derivative of the Fermi-Dirac distribution $[\cosh^2(\epsilon/2T)]^{-1} = -\partial f_F/\partial\epsilon$, the temperature $T$, and the energy $\epsilon$ (self-consistency is carried out by this variable). A detailed derivation of Eq. (1) in the general case is provided in the appendix of [23]. Other studies have also reported the use of a constant scattering lifetime [24], while other researchers have used a Fourier order parameter expansion to fit the experimental data in strontium ruthenate [25].

The ultrasound attenuation term $\alpha_j$ in Eq. (1) is derived from the imaginary part of the polarization operator [26,27], and has been used to study the anisotropic gap directional structure in conventional [28,29] and unconventional superconductors. It should be pointed out that it is instructive to compare with the heavy fermion compound $UPt_3$ [30–32] due to the evidence found from ultrasound studies of several superconducting phases, and the complicated structure of its Fermi surface.

On the other hand, other properties worth mentioning from the interaction of electrons and sound waves in strontium ruthenate are the splitting of the critical temperature in a uniaxial external stress field [33,34], the unusual power law behavior of the electron-phonon interaction in the $\alpha$, $\beta$ and $\gamma$ Fermi surfaces sheets below the transition temperature $T_c$ [21,22], the uncommon behavior of the normal state viscosity above $T_c$ [21,23], and the temperature power law activity due to different phonon modes [35].

The first unconventional compound to exhibit a jump at $T_c$ in one elastic velocity mode was the heavy fermion alloy $UPt_3$. It was the first superconductor to show a jump at $T_c$ in one elastic mode. This physical property has been interpreted as a signature of a broken symmetry [36,37]. In the case of $Sr_2RuO_4$, the first experimental discovery that shows a broken time-reversal symmetry is due to [3]. Theoretically, the velocity jump obtained using the Green function formalism is given by the real part of the polarization operator [27]. However, in the case of strontium ruthenate several experiments and calculations using the Gibbs thermodynamic potential $G(T)$ have been performed assuming an elastic broken symmetry field [38–42].

The other non-equilibrium property of interest, that is, the electronic thermal conductivity ($\kappa_i$) in the superconducting strontium ruthenate was experimentally measured in Ref. [43], and numerically calculated in Ref. [44] giving an excellent agreement with the fit performed. In this case, the use of a constant superconducting lifetime ratio is a key factor for a successful fitting. Therefore, the reason for the constant superconducting lifetime in this compound requires further research and is addressed in this study. It is worth mentioning, that for $\kappa_i$, two signatures are relevant: the universal behavior at very low temperatures, and the reduction of the transition temperature with non-magnetic disorder [45,46].

In the following two sections, we report a numerical analysis supporting our findings, *i.e.*, flat imaginary parts of the elastic scattering cross-section, concluding that a constant self-consistent superconducting lifetime is possible in strontium ruthenate for two different concentrations of stoichiometric disorder, when the disorder is dilute and near the unitary limit, and for enriched disorder in the intermediate scattering region.

## 2. Numerical procedure

The self-consistent Green-functions treatment of the frequency-dependent inverse scattering lifetime $\tau_s$ using rationalized Planck units ($\hbar = k_B = c = 1$) is performed using the expression [14]

$$\frac{1}{\tau_s(\omega)} = 2\,\Im\,[\,\tilde{\omega}\,(\,\omega + i0^+)\,]. \quad (3)$$

Equation (3) connects $\tau_s$ and the imaginary part of the elastic scatterings cross-section. The normal state lifetime $\tau_n$ is constant in normal metals, and therefore in strontium ruthenate since the compound is a robust Fermi liquid with three Fermi sheets [47]. Thus, a normal metal follows a simple lifetime equation $\tau_n^{-1} = C$, with a constant value.

Henceforth using Eq. (3), the ratio $\tau_s/\tau_n$ becomes equal to

$$\frac{\tau_s}{\tau_n} = \frac{C}{\Im(\,\tilde{\omega}\,)}.$$

Although, if the scattering lifetime also becomes constant in the superconducting state, we have that

$$\frac{1}{\tau_s} = C_s,$$

and the normal-superconducting lifetime ratio is a constant value that follows the expression

$$\frac{\tau_s}{\tau_n} = \text{constant}.$$

Nevertheless, it is physically significant to find as well, where the constituents quasiparticles of strontium ruthenate scatter mostly, that is, in the hydrodynamic, in the intermediate, in the unitary, or in between any of these elastic scattering phases, as further explained in the next section. This way we obtain the expression for the lifetime ratio using the expression of the imaginary part of the elastic cross-section that in non-equilibrium statistical thermodynamics is equivalent to half of the inverse scattering lifetime, and half of the collision frequency.

Additionally, We use a group theoretical expression for a triplet gap that breaks time-reversal symmetry, and it is consistent with the experiments mentioned for strontium ruthenate, that is, the Miyake-Narikiyo triplet order parameter [48]. it is worth mentioning other group theoretical models used to explain the nodal structure of $Sr_2RuO_4$, those models have an order parameter with line nodes, point nodes, or a combination of them, and also fit successfully experimental data. For example the superconducting specific heat [49–52].

The behavior of the pair of coordinates $(\Re(\tilde{\omega}), \Im(\tilde{\omega}))$ is analyzed for strontium ruthenate in the reduced phase space $(RPS)$ by sketching a phenomenological phase diagram [53]. The $RPS$ has two coordinates, the axis $0X$ is the real part of the self-consistent frequency, and the axis $0Y$ is its imaginary term. Besides, our numerical procedure controls five input physical parameters in the anisotropic case: the Fermi level $\epsilon_F$, the first tight binding hoping parameter $t$, the zero superconducting gap $\Delta_0$, the inverse scattering strength $c$, and the stoichiometric strontium disorder $\Gamma^+$.

As was pointed out in the introduction, strontium ruthenate is a triplet superconductor with $T_c \approx 1.5\,K$ and depends on the disorder. It belongs to the complex $2D$ irreducible representation $E_{2u}$ [33, 42]. The structure of the triplet gap is $\mathbf{\Delta}\ (k_x, k_y) = \Delta_0\ \mathbf{d}(\mathbf{k_x}, \mathbf{k_y})$, where the order parameter vector is given by the expression $\mathbf{d}\ (k_x, k_y) = [\sin(k_x a) + i\ \sin(k_y a)]\,\mathbf{z}$. The zero gap parameter in this work takes values from 0.0 meV in the normal state to the threshold experimental value of 1.0 meV.

The numerical solution containing the dependent self-consistent frequency that changes quickly and it is found on both sides of the following self-consistent equation [54, 55]

$$\tilde{\omega}\ (\ \omega\ + i\,0^+) = \omega + i\ \pi\ \Gamma^+\ \frac{g(\tilde{\omega})}{c^2 + g^2(\tilde{\omega})}. \qquad (4)$$

The numerical disorder is controlled in the imaginary part of the (4) with the help of two parameters, the inverse scattering strength $c$, and the stoichiometric strontium disorder $\Gamma^+$ [54, 55]. The dimensionless inverse strength parameter $c = 1/(\pi\, N_F\, U_0)$, where $U_0$ is the atomic disorder potential and $N_F$ is the density of states at the Fermi level. The other parameter is the strontium stoichiometric disorder concentration $\Gamma^+ = n_{\text{imp}}/(\pi^2\, N_F)$. The expression that gives the function $g(\tilde{\omega})$ is

$$g(\tilde{\omega}) = \left\langle \frac{\tilde{\omega}}{\sqrt{\tilde{\omega}^2 - |\Delta|^2(k_x, k_y)}} \right\rangle_{FS}.$$

The isotropic Fermi surface approach to Eq. (4) with the disorder parameters $c$, and $\Gamma^+$ is summarized in Ref. [56]. Still, concerning the scattering cross-section approach, we can use a tight-binding anisotropic model for the $HTSC$ strontium-doped lanthanum cuprate [57] and strontium ruthenate [8]. It is important to notice that strontium ruthenate is found with quasi-point nodes or point node order parameter structures by only changing the value of the Fermi level [15]. However, in this study, the Fermi level is 0.4 meV, the first neighbor hoping parameter is 0.4 meV, and the normal state energy expression is $\xi(k_x, k_y) = -\epsilon_F + 2t\ [\cos(k_x a) + \cos(k_y a)]$ which correspond to a quasi-point nodal structure.

Thus, the Fermi level value $\epsilon_F = 0.4$ meV makes the normal state energy anisotropic and leaves a quasi-point tiny gap around the $(0, \pm\pi)$ and $(\pm\pi, 0)$ points [48]. The order parameter $\mathbf{d}(\mathbf{k_x}, \mathbf{k_y})$ has two components that belong to the irreducible representation $E_{2u}$ of the tetragonal point group $D_{4h}$. It corresponds to a triplet odd paired state $\mathbf{d}$ $(-k_x, -k_y) = -\mathbf{d}(\mathbf{k_x}, \mathbf{k_y})$ with a complex irreducible representation composed by the functions $\sin(k_x a)$ and $\sin(k_y a)$ and the Ginzburg-Landau coefficients $(1, i)$ [33, 42].

If $c = 0.0$, the Eq. (4) is in the unitary limit and given accordingly to [14]

$$\tilde{\omega}\big(\omega + i0^+\big) = \omega + i\ \pi\ \Gamma^+ \frac{1}{g(\tilde{\omega})},$$

where stoichiometric disorder $\Gamma^+$ is left as a unique parameter.

For this particular self-consistent simulation, we use two expressions: Subsection one of the next section is computed with a dilute disorder imaginary expression (5) between the unitary and intermediate regions

$$\tilde{\omega}\big(\omega + i0^+\big) = \omega + 0.05\ \pi\ \text{meV}\ \frac{g(\tilde{\omega})}{(0.2)^2 + g^2(\tilde{\omega})}. \qquad (5)$$

Subsection two of the next section is calculated using the Eq. (6) with an intermediate scattering and enriched disorder values according to

$$\tilde{\omega}\big(\omega + i0^+\big) = \omega + 0.2\ \pi\ \text{meV}\ \frac{g(\tilde{\omega})}{(0.4)^2 + g^2(\tilde{\omega})}. \qquad (6)$$

In what follows, simulations for the zero gap are performed in this case with the parameters $c = 0.2$, $c = 0.4$, a dilute stoichiometric disorder $\Gamma^+ = 0.05$ meV, and the enriched stoichiometric disorder $\Gamma^+ = 0.20$ meV as pointed out in Eqs. (5) and (6). Other values of $\Gamma^+$ for $c = 0.2$ are also compared, $\Gamma^+ = 0.10$ meV, and $\Gamma^+ = 0.15$ meV, both of them considered in the range of an optimal disorder. Additionally, we use eleven values for the zero superconducting gap $\Delta_0$ in each case, starting from the normal state ($\Delta_0 = 0.0$ meV), and adding 0.1 meV to each zero gap value. The threshold limit is the experimental value for strontium ruthenate ($\Delta_0 = 1.0$ meV), as this value shows a single tiny gap in the unitary limit.

## 3. Numerical results

### 3.1. Dilute disordered constant superconducting lifetime

In Subsec. 3.1, Fig. 1 shows the behavior of dressed fermionic carriers for which a constant scattering lifetime is observed in two regions of the reduced phase space and it is

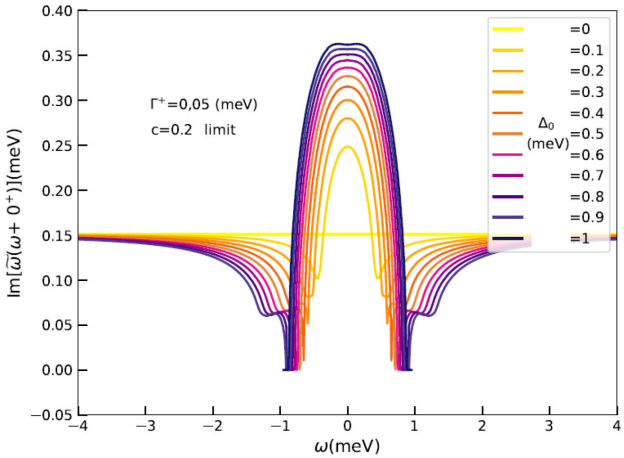


FIGURE 1. Evolution of the zero superconducting gap for $c = 0.2$ and dilute disorder in strontium ruthenate. This plot is flat at real frequency intervals $\pm(0.00, 0.26)$ meV. Also, notice several tiny gaps for $\Delta_0 = 0.8$, 0.9, and 1.0 meV.

calculated using Eq. (5). The first interval is the normal state phase with real frequencies between $\pm\,(3.1, 4.0)$ meV and a constant imaginary frequency $\Im\,(\tilde{\omega}) = 0.149$ meV. The second interval is localized inside the superconducting phase and shows a superconducting scattering lifetime constant for real frequencies in the interval $\pm\ (0.0, 0.26)$ meV (see Table II for a numerical sample of the numbers in the superconducting case). The superconducting zero gap parameters in Fig. 1 correspond to the values $\Delta_0 = 0.0$ (normal state), and $\Delta_0 = (0.1, 0.2, 0.3, 0.4, 0.5, 0.6, 0.7, 0.8, 0.9, 1.0)$ meV (the last is the threshold value).

Since the function $\Im\ (\tilde{\omega})$ is constant, it corresponds to a constant scattering lifetime in the superconducting state of strontium ruthenate, confirming the general prediction of a constant lifetime ratio for unconventional superconductors [16], and the fittings of experimental data for $\alpha$ and $\kappa$ [22, 44]. We show in Table II, a sample of the real, and the imaginary $RPS$ coordinates with the flat shape in Fig. 1. This happens for $c = 0.2$, which means outside the unitary and the intermediate limits, with a dilute stoichiometric disorder value given by $\Gamma^+ = 0.05$ meV. Three microscopic zero superconducting gap values are shown in Table II: $\Delta_0 = 0.8$, 0.9, 1.0 meV.

From Fig. 1 and Table II, we find that the superconducting $\Im\ (\tilde{\omega})$ has a value of $0.362$ meV, bigger than the value $\Im\ (\tilde{\omega}) = 0.149$ meV in the normal state. That means that the constant scattering lifetime is smaller in the superconducting dilute disorder phase. The superconducting collision frequency is bigger than in its normal state, probably due to the existence of scattering processes coming from other dressed fermions, and the phonon quasiparticles (sound waves) with the strontium-disordered atoms. We think that for the unconventional strontium ruthenate at low frequencies, the momentum of the dressed quasiparticles is transferred to strontium stoichiometric disordered atoms in the crystal lattice, contrary to what happens in the high $T_c$ lightly doped lanthanum cuprate $La_{2-x}Sr_xCuO_4$, where the $k$-transfer happens at higher or much higher frequencies in the unitary limit, and it becomes harder to find the frequency point of the phase transition in the $RPS$ [58]. A simple physical picture tells us that $Sr$ atoms migrate through the lattice, and stick together in a coalescing metallic state with a constant lifetime, but this time it happens for a dilute disorder of stoichiometric $Sr$ atoms ($\Gamma^+ = 0.05$ meV) and low frequencies (if a species of an atom is stoichiometric, an infinite unitary $U_0$ is not needed to form a coalescent metallic phase).

Another geometrical feature in Fig. 1 for frequencies just below the phase transition happens with zero gap values of $0.8, 0.9,$ and $1.0$ meV, where the tiny gap is stimulated if $c = 0.2$, meaning that if the zero superconducting gap value is increased close to the threshold value by 0.1 meV steps, the tiny gap produces a region with only boson super-carriers. It is interesting to notice how the tiny gap in the imaginary part becomes smaller, as $\Delta_0$ decreases. Thus, in Fig. 1 with the inverse strength parameter $c = 0.2$, we observe a tiny gap shaping up in the superconducting phase. This feature in Fig. 1 is supported by a sample of numbers in Table III.

We remark that the tiny gaps in the cases studied remain positive as can be seen in Table III, and the 0Y axis is extended in Fig. 1 to negative values to visualize that in the $RPS$ it follows the rule $\Im\ (\tilde{\omega}) > 0.0$ meV. Finally in Fig. 1 is noticed that the tiny gap at $c = 0.2$ and $\Gamma^+ = 0.05$ meV for $\Delta_0 = 1.0$ meV does not display numbers in the normal state (see the last column of Table III).

TABLE II. Sample of real and imaginary $RPS$ frequencies and different zero gaps (all values are in meV units) for $c = 0.2$ with dilute disorder.

| | | | | | | | | | |
|---|---|---|---|---|---|---|---|---|---|
| $\Re\,(\tilde{\omega})$ | $1.0\,e^{-3}$ | $2.1\,e^{-2}$ | $4.1\,e^{-2}$ | $7.1\,e^{-2}$ | $1.01\,e^{-1}$ | $1.31\,e^{-1}$ | $1.51\,e^{-1}$ | $1.81\,e^{-1}$ | $2.61\,e^{-1}$ |
| $\Im\,(\tilde{\omega})$ $\Delta_0 = 1.0$ | $3.62\,e^{-1}$ | $3.62\,e^{-1}$ | $3.62\,e^{-1}$ | $3.62\,e^{-1}$ | $3.62\,e^{-1}$ | $3.62\,e^{-1}$ | $3.62\,e^{-1}$ | $3.62\,e^{-1}$ | $3.60\,e^{-1}$ |
| $\Im\,(\tilde{\omega})$ $\Delta_0 = 0.9$ | $3.57\,e^{-1}$ | $3.57\,e^{-1}$ | $3.57\,e^{-1}$ | $3.57\,e^{-1}$ | $3.57\,e^{-1}$ | $3.57\,e^{-1}$ | $3.56\,e^{-1}$ | $3.56\,e^{-1}$ | $3.55\,e^{-1}$ |
| $\Im\,(\tilde{\omega})$ $\Delta_0 = 0.8$ | $3.51\,e^{-1}$ | $3.51\,e^{-1}$ | $3.51\,e^{-1}$ | $3.51\,e^{-1}$ | $3.51\,e^{-1}$ | $3.50\,e^{-1}$ | $3.50\,e^{-1}$ | $3.49\,e^{-1}$ | $3.44\,e^{-1}$ |

TABLE III. Real and imaginary tiny gap numbers in the $RPS$ for different zero gaps (all values in meV) with dilute disorder and two scattering regions.

| | | | | | | |
|---|---|---|---|---|---|---|
| $\Re\,(\tilde{\omega})$ | $7.01\,e^{-1}$ | $8.01\,e^{-1}$ | $8.51\,e^{-1}$ | $9.01\,e^{-1}$ | $9.51\,e^{-1}$ | $1.00\,e^{+0}$ |
| $\Im\,(\tilde{\omega})$ $\Delta_0 = 1.0$ $c = 0$ | $2.27\,e^{-1}$ | $8.17\,e^{-2}$ | $8.63\,e^{-7}$ | $2.21\,e^{-8}$ | $5.57\,e^{-5}$ | $4.41\,e^{-2}$ |
| $\Im\,(\tilde{\omega})$ $\Delta_0 = 1.0$ $c = 0.2$ | $2.46\,e^{-1}$ | $1.66\,e^{-1}$ | $9.28\,e^{-2}$ | $5.14\,e^{-6}$ | $6.12\,e^{-8}$ | – |
| $\Im\,(\tilde{\omega})$ $\Delta_0 = 0.9$ $c = 0.2$ | $2.26\,e^{-1}$ | $1.32\,e^{-1}$ | $3.37\,e^{-3}$ | $8.12\,e^{-5}$ | $4.50\,e^{-2}$ | $5.81\,e^{-2}$ |

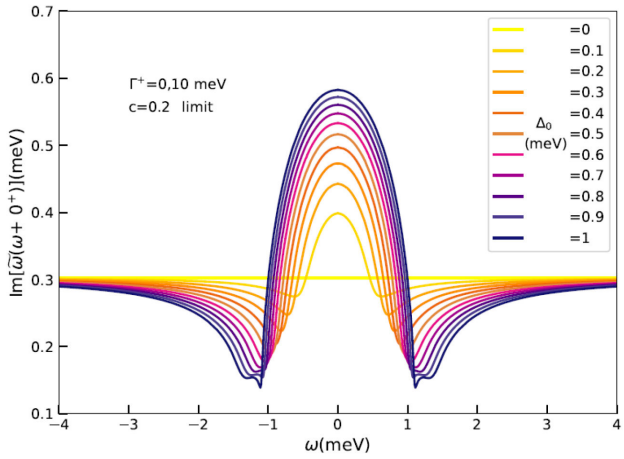


FIGURE 2. Evolution of the zero superconducting gap for $c = 0.2$ and quasi-optimal disorder in strontium ruthenate.

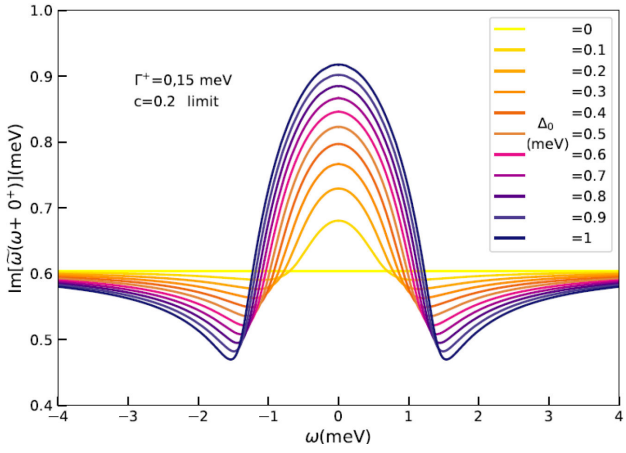


FIGURE 3. Evolution of the zero superconducting gap for $c = 0.2$ and optimal disorder in strontium ruthenate.

Two additional simulations with a set of parameters $c = 0.2$ and $\Gamma^+ = 0.10$ meV, and $c = 0.2$ and $\Gamma^+ = 0.15$ meV, that is, quasi-optimal and optimal disorder, show similar behavior as for the unitary limit [60], with a maximum zero real frequencies, and an imaginary minimum that decreases as $\Delta_0$ takes smaller values. Figures 2 and 3 show how the zero gap transition smoothly decreases. For example, we notice from Fig. 2 that only for the value $c = 0.2$, $\Gamma^+ = 0.10$ meV, and $\Delta_0 = 1.0$ meV (dark blue plot) there is a sharp minimum but the tiny gap does not shape up as in Fig. 1. We also observe that the transition point is a smooth function in most cases which says about non-locality in strontium ruthenate, and changes the position and the slope, as $\Delta_0$ increases. We think, that this feature belongs to triplet superconductors that break the time-reversal symmetry.

### 3.2. Enriched doped constant superconducting lifetime

In Subsec. 3.2, Fig. 4 addresses the existence of a different stoichiometric disorder for a constant superconducting lifetime that is settled self-consistently. The issue is answered by modeling the intermediate regime for strontium ruthenate $(c = 0.4)$ and varying the zero gap from the normal state

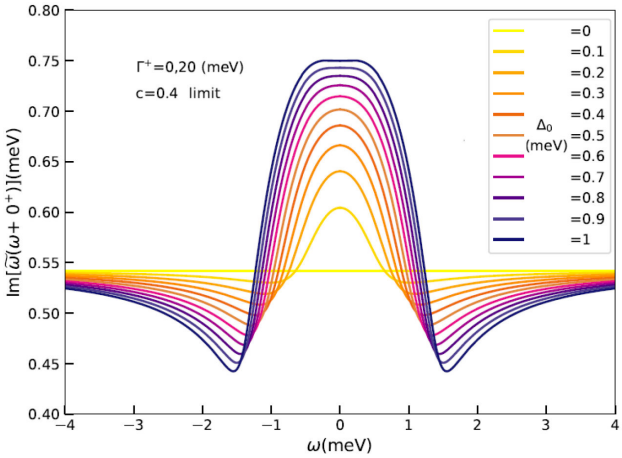


FIGURE 4. Evolution of the zero superconducting gap for $c = 0.4$ and enriched disorder in strontium ruthenate. This plot is flat at real frequency intervals $\pm(0.00, 0.36)$ meV for $\Delta_0 = 0.9$ and 1.0 meV.

TABLE IV. Sample of real and imaginary frequencies, and different zero gaps (all values in meV units) for $c = 0.4$ and an enriched disorder.

| | | | | | | | | | |
|---|---|---|---|---|---|---|---|---|---|
| $\Re(\tilde{\omega})$ | $1\,e^{-3}$ | $2.1\,e^{-2}$ | $4.01\,e^{-2}$ | $7.10\,e^{-2}$ | $1.01\,e^{-1}$ | $1.31\,e^{-1}$ | $1.51\,e^{-1}$ | $1.81\,e^{-1}$ | $3.61\,e^{-1}$ |
| $\Im(\tilde{\omega})$ | $7.49\,e^{-1}$ | $7.49\,e^{-1}$ | $7.49\,e^{-1}$ | $7.49\,e^{-1}$ | $7.50\,e^{-1}$ | $7.50\,e^{-1}$ | $7.50\,e^{-1}$ | $7.50\,e^{-1}$ | $7.48\,e^{-1}$ |
| $\Delta_0 = 1.0$ | | | | | | | | | |
| $\Im(\tilde{\omega})$ | $7.43\,e^{-1}$ | $7.42\,e^{-1}$ | $7.42\,e^{-1}$ | $7.42\,e^{-1}$ | $7.42\,e^{-1}$ | $7.42\,e^{-1}$ | $7.42\,e^{-1}$ | $7.42\,e^{-1}$ | $7.38\,e^{-1}$ |
| $\Delta_0 = 0.9$ | | | | | | | | | |
| $\Im(\tilde{\omega})$ | $7.35\,e^{-1}$ | $7.34\,e^{-1}$ | $7.34\,e^{-1}$ | $7.34\,e^{-1}$ | $7.34\,e^{-1}$ | $7.34\,e^{-1}$ | $7.34\,e^{-1}$ | $7.33\,e^{-1}$ | $7.28\,e^{-1}$ |
| $\Delta_0 = 0.8$ | | | | | | | | | |

value to the threshold limit, with an enriched stoichiometric disorder given by $\Gamma^{+} = 0.20$ meV in Eq. (6). Figure 4 shows that in that particular case, a robust flat imaginary cross-section develops inside the superconducting phase for the real frequency interval $\pm(0.00, 0.36)$ meV.

Therefore, in Table IV, we present a sample of the numbers calculated. We find that $\Im(\tilde{\omega}) = 0.749$ meV. This case shows that the real frequency interval with a constant superconducting scattering lifetime decreases as $\Delta_0$ is reduced by 0.1 meV steps. The sample of the values reported in Table IV supports Fig. 4, and they are calculated using an enriched stoichiometric disorder represented by $\Gamma^{+} = 0.20$ meV. To end this section, we think that the last outcome seems to be a general feature of the elastic scattering cross-section in triplet superconductors with a smooth transition where the disorder is induced by stoichiometric $Sr$ atoms.

## 4. Conclusions

This work aimed to introduce some numerical examples with a constant scattering self-consistent lifetime in the unconventional superconductor strontium ruthenate, and it is inspired by the experimental research work [59]. A singular phase that shows an imaginary elastic scattering cross-section with a single value for an interval of real frequencies in the $RPS$ is found for two scattering limits. The importance of this numerical finding relies on its use, as it justifies the experimental fits of the non-equilibrium experimental data.

Thus, in the simulation of the Fig. 1 and the Table II, it was analyzed a limit with the strength fixed at $c = 0.2$, and a stoichiometric dilute disorder $\Gamma^{+} = 0.05$ meV (standing in between the unitary and the intermediate regimes). The set of real frequencies for which the lifetime is constant is found in the interval $(0.00, 0.26)\,meV$ and a value of $\Im(\tilde{\omega})$ = 0.362 meV. This gives a value of 0.181 meV for the superconducting collision frequency $\nu$, and a value of $0.764\,meV$ for the inverse scattering superconducting lifetime. These three values can be contrasted with those of the normal metallic state (with a Fermi liquid behavior) also found in the Fig. 1 and the Table II, where $\Im(\tilde{\omega}) = 0.149$ meV, $\nu = 0.075$ meV, and an inverse normal lifetime value of 0.298 meV. We notice that the collision superconducting frequency doubles the normal state collision frequency for a considerable atomic $Sr$ potential strength $U_0 \gg 1$, despite the fact, that the lifetime is constant in both phases, and the disorder concentration of $Sr$ atoms is diluted.

We also studied a limit with the strength fixed at intermediate regimen, *i.e.*, $c = 0.4$, and an enriched stoichiometric disorder $\Gamma^{+} = 0.20$ meV. A broader $\pm(0.00, 0.36)$ meV interval of real frequencies throws a constant $\Im(\tilde{\omega}) = 0.749$ meV. The superconducting collision frequency is calculated to be $\nu = 0.382$ meV, and a value of 1.528 meV is obtained for the inverse superconducting scattering lifetime. These three values can be compared in the Fig. 4 and the Table IV with its normal metallic state where $\Im(\tilde{\omega}) = 0.524$ meV, $\nu = 0.262$ meV, and $\tau_n^{-1} = 1.048$ meV. We notice how for an enriched stoichiometric disorder, the collision superconducting frequency increases when compared to the value having a dilute disorder in Fig. 1 and Table II. This finding remarks the role of strontium atoms in the elastic scattering process when disorder is considered.

Therefore, we can state that some self-consistent computations using an order parameter with the irreducible representation $E_{2u}$ find that:

- An state with strength $c = 0.2$ and dilute disorder shows several tiny gaps (Fig. 1 and Table III), contrasting the unitary Miyake-Narikiyo case with $c = 0.0$ and the same dilute disorder that shows a single tiny gap.
- The ratio of the normalized ultrasound attenuation in the dilute disorder case is proportional to the constant value $0.390$ (Fig. 1 and Table II).
- The ratio of the normalized ultrasound attenuation in the enriched disorder case is proportional to the constant value $0.686$ (Fig. 4 and Table IV).

We focused our study outside the unitary regime. However, a set of calculations in the unitary limit varying the zero gap was performed in Ref. [60], to study other physical properties of strontium ruthenate.

The arguments sketched in the previous paragraphs help to understand the physics of disordered strontium ruthenate [7], where research about its superconducting nature is still growing despite it was discovered 30 years ago. Some new interesting directions in strontium ruthenate and similar

compounds such as strontium ferrite under pressure are mentioned in Ref. [61]. In references [62–64] and works therein, other properties of importance for strontium ruthenate as the nature of the order parameter are discussed in detail. We finally mention a non-locality discussion comparing the compounds palladium-cobalt delafossite and strontium ruthenate [65]. Other properties in several families of superconducting unconventional alloys such as heavy fermions are addressed in the monograph [66], and an interesting mechanism for changing $T_c$ with fluctuations is studied in Ref. [67].

## Acknowledgments

We thank an anonymous reviewer for the useful insights to improve the structure and grammar of this work.

**Authorship contribution statement**

Pedro Contreras: Conceptualization, Methodology, Software, Investigation, Validation, writing-original draft, Supervision, Writing-review and editing.

**Declaration of competing interest**

The author declares that he has no known competing financial interests or personal relationships that could have appeared to influence the work reported in this paper.


1. Y. Maeno *et al.*, Superconductivity in a layered perovskite without copper, *Nature* **372** 532, https://doi.org/10.1038/372532a0
2. T. Rice and M. Sigrist, $Sr_2RuO_4$: an electronic analogue of 3He?, *Journal of Physics: Condensed Matter* **7**(47) (1995) L643
3. G. Luke *et al.*, Time-reversal symmetry-breaking superconductivity in $Sr_2RuO_4$, *Nature* **394**(6693) (1998) 558, https://doi.org/10.1038/29038
4. K. Ishida *et al.*, Spin-triplet superconductivity in $Sr_2RuO_4$ identified by $^{17}O$ Knight shift. *Nature* **396** (1998) 658, https://doi.org/10.1038/25315
5. J. Duffy *et al.*, Polarized-neutron scattering study of the Cooper-pair moment in $Sr_2RuO_4$, *Phys. Rev. Lett.* **85**(25) (2000) 5412, https://doi.org/10.1103/PhysRevLett.85.5412
6. F. Laube, G. Goll, H. Lohneysen, M. Fogelstrom, and F. Lichtenberg, Spin-Triplet Superconductivity in $Sr_2RuO_4$ Probed by Andreev Reflection, *Phys. Rev. Lett.* **84** (2000) 1595, https://doi.org/d10.1103/PhysRevLett.84.1595
7. A. Mackenzie *et al.*, Extreme dependence of superconductivity on the disorder in $Sr_2RuO_4$, *Phys. Rev. Lett.* **80** (1998) 161, https://doi.org/10.1103/PhysRevLett.80.161
8. P. Contreras, D. Osorio, and S. Ramazanov, Nonmagnetic tight-binding effects on the $\gamma$ sheet of $Sr_2RuO_4$, *Rev. Mex. Fis.* **68**(2) (2022) 020502, https://doi.org/10.31349/RevMexFis.68.020502
9. V. Ambegaokar and A. Griffin, Theory of the thermal conductivity of superconducting alloys with paramagnetic impurities, *Phys. Rev.* **137**(4A) (1965) A1151, https://doi.org/10.1103/PhysRev.137.A1151
10. C. Pethick, and D. Pines, Transport processes in heavy-fermion superconductors, *Phys. Rev. Lett.* **57**(1) (1986) 118, https://doi.org/10.1103/PhysRevLett.57.118
11. P. Hirschfeld, P. Wölfle, and D. Einzel, Consequences of resonant impurity scattering in anisotropic superconductors: Thermal and spin relaxation properties, *Phys. Rev. B.* **37**(1) (1988) 83, https://doi.org/10.1103/PhysRevB.37.8
12. B. Arfi and C. Pethick, Thermal conductivity and ultrasonic attenuation in heavy fermion superconductors, *Phys. Rev. B.*, **38** (1988) 2312, https://doi.org/10.1103/PhysRevB.38.2312
13. A. Balatsky, M. Salkola, and A. Rosengren, Impurity-induced virtual bound states in d-wave superconductors, *Phys. Rev. B.* **51**(21) (1995) 15547, https://doi.org/10.1103/physrevb.51.15547
14. V. Mineev, and K. Samokhin, Introduction to Unconventional Superconductivity (Gordon and Breach Science Publishers, 1999)
15. P. Contreras, D. Osorio, and S. Tsuchiya, Quasi-point versus point nodes in $Sr_2RuO_4$, the case of a flat tight binding $\gamma$ sheet, *Rev. Mex. Fis.* **68**(6) (2002) 060501, https://doi.org/10.31349/RevMexFis.68.060501
16. S. Schmitt-Rink, K. Miyake, and C. Varma, Transport and thermal properties of heavy-fermion superconductors: A unified picture, *Phys. Rev. Lett.* **57** (1986) 2575, https://doi.org/10.1103/PhysRevLett.57.2575
17. F. Reif, Fundamentals of Statistical and Thermal Physics, (McGraw Hill, 1965, ISBN 0-07-051800-9)
18. I. Kvashnikov, The Theory of Systems out of Equilibrium, (Moscow State University Press, 2003).
19. J. W. Daily, Statistical Thermodynamics, an Engineering Approach, (Cambridge University Press, 2019) https://doi.org/10.1017/9781108233194
20. R. Jansen, F. Behnam, and M. Kelly, The steady-state self-consistent solution to the nonlinear Wigner-function equation; a new approach, *Physica B: Condensed Matter*, **175**(1-3) (1991) 49, https://doi.org/10.1016/0921-4526(91)90688-B
21. C. Lupien, W. A. MacFarlane, C. Proust, L. Taillefer, Z. Q. Mao, and Y. Maeno, Ultrasound attenuation in $Sr_2RuO_4$: An angle-resolved study of the superconducting gap function, *Phys. Rev, Lett.* **86**(26) (2001) 5986, https://doi.org/10.1103/PhysRevLett.86.5986

22. P. Contreras, M. B. Walker, and K. Samokhin, Determining the superconducting gap structure in $Sr_2RuO_4$ from sound attenuation studies below $T_c$. *Phys. Rev. B.* **70**(18) (2004) 184528, https://doi.org/10.1103/PhysRevB.70.184528

23. M. B. Walker, M. Smith, and K. Samokhin, Electron-phonon interaction and ultrasonic attenuation in the ruthenate and cuprate superconductors, *Phys. Rev. B.* **65**(1) (2001) 014517, https://doi.org/10.1103/PhysRevB.65.014517

24. WC. Wu, and R. Joynt, Transport and the order parameter of superconducting $Sr_2RuO_4$, *Phys. Rev. B.* **64**(10) (2001) 100507, https://doi.org/10.1103/PhysRevB.64.100507

25. T. Nomura, Theory of transport properties in the p-wave superconducting state of $Sr_2RuO_4$ a microscopic determination of the gap structure, *J. Phys. Soc. Jpn.* **74**(6) (2005) 1818, https://doi.org/10.1143/jpsj.74.1818

26. I. O. Kulik, Heat anomaly of superconductors, *JETP*. **16**(4) (1963) 1952. ISSN: 0044-4510

27. V. Vaskin, and V. Demikhovskii, Sound dispersion in superconducting semiconductors, *Soviet Physics of the Solid State* **10**(2) (1968) 330 ISSN: 0038-5654

28. R. Dobbs, and J. Perz, Anisotropy of the Energy Gap in Niobium from Ultrasonic Measurements, *Rev. Mod. Phys.* **36** (1964) 257 https://doi.org/10.1103/RevModPhys.36.257

29. V. Pokrovskii and V. Toponogov, Reconstruction of the energy gap in a superconductor by measurement of sound attenuation, *JETP* **13**(4) (1961) 785 ISSN: 0044-4510

30. D. Hess, T. Tokuyasu and J. Sauls, Broken symmetry in an unconventional superconductor: a model for the double transition in $UPt_3$, *J. Phys.: Condens. Matter* **1** (1989) 8135, https://doi.org/10.1088/0953-8984/1/43/014

31. B. Shivaram, Y. Jeong, T. Rosenbaum and D. Hinks, Anisotropy of transverse sound in the heavy-fermion superconductor $UPt_3$, *Phys. Rev. Lett.* **56** (1986) 1078, https://doi.org/10.1103/PhysRevLett.56.1078

32. R. Joynt and L. Taillefer, The superconducting phases of $UPt_3$, *Rev. of Modern Physics*, **74** (2002) 235, https://doi.org/10.1103/RevModPhys.74.235

33. M. B. Walker and P. Contreras, Theory of elastic properties of $Sr_2RuO_4$ at the superconducting transition temperature, *Phys. Rev. B.* **66**(21) (2002) 214508, https://doi.org/10.1103/PhysRevB.66.214508

34. M. Sigrist, Ehrenfest relations for ultrasound absorption in $Sr_2RuO_4$, *Progress of Theoretical Physics* **107**(5) (2002) 917, https://doi.org/10.1143/PTP.107.917

35. J . Moreno and P. Coleman, Ultrasound attenuation in gap-anisotropic systems. *Phys. Rev. B.* **53** (1996) R2995, https://doi.org/10.1103/PhysRevB.53.R2995

36. G. Bruls, D. Wever, B. Wolf, P. Thalmeier and B. Luthi, Strain order parameter coupling and phase diagrams in superconducting $UPt_3$. *Phys. Rev. Lett.*, **65** (1990) 2294, https://doi.org/10.1103/PhysRevLett.65.2294

37. S. Adenwalla, *et al.*, 1990. Phase diagram of $UPt_3$ from ultrasonic velocity measurements. Phys. Rev. Lett., 65:2298. https://doi.org/10.1103/PhysRevLett.65.2298

38. C. Hicks *et al.*, Strong increase of $T_c$ of $Sr_2RuO_4$ under both tensile and compressive strain, *Science* **344**(6181) (2014) 283, https://doi.org/10.1126/science.1248292

39. S. Benhabib *et al.*, Ultrasound evidence for a two-component superconducting order parameter in $Sr_2RuO_4$, *Nature Physics* (2020) 6 https://doi.org/10.1038/s41567-020-1033-3

40. S. Ghosh *et al.*, 2020. Thermodynamic evidence for a two-component superconducting order parameter in $Sr_2RuO_4$, *Nature Physics* (2020) 9, https://doi.org/10.1038/s41567-020-1032-4

41. V. Grinenko *et al.*, Unsplit superconducting and time-reversal symmetry breaking transitions in $Sr_2RuO_4$ under hydrostatic pressure and disorder, *Nat. Commun.* **12**, (2021) 3920, https://doi.org/10.1038/s41467-021-24176-8

42. P. Contreras, J. Florez, and R. Almeida, Symmetry field breaking effects in $Sr_2RuO_4$, *Rev. Mex. Fis.* **62**(5) (2016) 442, ISSN: 2683-2224

43. M. Tanatar, S. Nagai, ZQ. Mao, Y. Maeno and T. Ishiguro, 2001. Thermal conductivity of superconducting $Sr_2RuO_4$ in oriented magnetic fields, *Phys. Rev. B.* **63**(6) (2001) 064505, https://doi.org/10.1103/PhysRevB.63.064505

44. P. Contreras, Electronic heat transport for a multiband superconducting gap in $Sr_2RuO_4$, *Rev. Mex. Fis.* **57**(5) (2011) 395, ISSN: 2683-2224

45. M. Suzuki, M. Tanatar, N. Kikugawa, ZQ. Mao, Y. Maeno and T. Ishiguro, Universal heat transport in $Sr_2RuO_4$. *Phys. Rev. Lett.* **88** (2002) 227004, https://doi.org/10.1103/PhysRevLett.88.227004

46. A. Larkin, Vector pairing in superconductors of small dimensions, *JETP Letters* **2**(5) (1965) 105, ISSN: 0370-274X

47. C. Bergemann, S. Julian, A. Mackenzie, S. Nishizaki and Y. Maeno, Detailed topography of the Fermi surface of $Sr_2RuO_4$, *Phys. Rev. Lett.* **84** (2000) 2662, https://doi.org/10.1103/PhysRevLett.84.2662

48. K. Miyake and O. Narikiyo, Model for unconventional superconductivity of $Sr_2RuO_4$, the effect of impurity scattering on time-reversal breaking triplet pairing with a tiny gap, *Phys. Rev. Lett.* **83** (1999) 1423, https://doi.org/10.1103/PhysRevLett.83.1423

49. D. Agterberg, T. Rice and M. Sigrist, Orbital-dependent superconductivity in $Sr_2RuO_4$, *Phys. Rev. Lett.* **78** (1997) 3374, https://doi.org/10.1103/PhysRevLett.78.3374

50. M. Zhitomirsky and T. Rice, Interband proximity effect and nodes of the superconducting gap in $Sr_2RuO_4$, *Phys. Rev. Lett.* **87**(5) (2001) 057001, https://doi.org/10.1103/PhysRevLett.87.057001

51. K. Deguchi, Z. Mao, H. Yaguchi and Y. Maeno, Gap structure of the spin-triplet superconductor $Sr_2RuO_4$ determined from the field-orientation dependence of the specific heat, *Phys. Rev. Lett.* **92** (2004) 047002, https://doi.org/10.1103/PhysRevLett.92.047002

52. K. Wysokinski, G. Litak, J. Annett, and B. Gyorffy. Spin triplet superconductivity in $Sr_2RuO_4$, *Phys. Stat. Sol (b)*, **236** (2003) 325, https://doi.org/10.1002/pssb.200301672

53. P. Contreras, The collision frequency in two unconventional superconductors, *Can. J. Pure Appl. Sci.* **17**(3) (2023) 5731, ISSN: 1920-3853

54. E. Schachinger, and JP. Carbotte, Residual absorption at zero temperature in d-wave superconductors, *Phys. Rev. B.* **67**(13) (2003) 134509, https://doi.org/10.1103/PhysRevB.67.134509

55. I. Schurrer, E. Schachinger, and J. P. Carbotte, Optical conductivity of superconductors with mixed symmetry order parameters *Physica C*, **303** (1998) 287, https://doi.org/10.1016/S0921-4534(98)00256-1

56. P. Contreras, and J. Moreno, A nonlinear minimization calculation of the renormalized frequency in dirty d-wave superconductors, *Can. J. Pure Appl. Sci.* **13**(2) (2019) 4765, ISSN: 1920-3853

57. P. Contreras and D. Osorio, Scattering due to non-magnetic disorder in 2D anisotropic d-wave high $T_c$ superconductors, *Engineering Physics* **5**(1) (2021) 1, https://doi.org/10.11648/j.ep.20210501.11

58. P. Contreras, D. Osorio, and A. Devi, Self-Consistent Study of the Superconducting Gap in the Strontium-doped Lanthanum Cuprate, *Int. J. Appl. Math. Theor. Phys.* **9**(1) (2023) 1, https://doi.org/10.11648/j.ijamtp.20230901.11

59. C. Lupien, Ultrasound attenuation in the unconventional superconductor $Sr_2RuO_4$, (Ph.D. thesis, University of Toronto, Toronto, Canada, 2002) https://hdl.handle.net/1807/120313

60. P. Contreras, D. Osorio, and A. Devi, The effect of nonmagnetic disorder in the superconducting energy gap of strontium ruthenate, *Physica B: Condensed Matter.* **646** (2022) 414330, https://doi.org/10.1016/j.physb.2022.414330

61. A. Kazemi-Moridani *et al.*, Strontium ferrite under pressure: Potential analog to strontium ruthenate, *Phys. Rev. B* **109** (2024) 165146, https://doi.org/10.1103/PhysRevB.109.165146

62. A. Leggett, and Y. Liu, Y, Symmetry Properties of Superconducting Order Parameter in $Sr_2RuO_4$, *J Supercond Nov Magn* **34** (2021) 1647, https://doi.org/10.1007/s10948-020-05717-6

63. S. Käser, Response functions of strongly correlated electron systems: From perturbative to many-body techniques. (Ph. D. Thesis, Friedrich-Alexander-Universität, Erlangen-Nürnberg, Germany, 2021)

64. A. Steppke *et al.*, Upper critical field of $Sr_2RuO_4$ under in-plane uniaxial pressure *Phys. Rev. B* **107** (2024) 064509, https://doi.org/10.1103/PhysRevB.107.064509

65. G. Baker *et al.*, Nonlocal Electrodynamics in Ultrapure $PdCoO_2$. *Phys. Rev. X* **14** (2024) 011018, https://doi.org/10.1103/PhysRevX.14.011018

66. J. Shaginyan, and M. Amusia, Strongly Correlated Fermi Systems: A New State of Matter (Springer Tracts in Modern Physics, 2020) https://doi.org/10.1007/978-3-030-50359-8

67. A. Krasavin *et al.*, Suppression of Superconducting Fluctuations in Multiband Superconductors as a Mechanism for Increasing the Critical Temperature (Brief Review) *JETP Lett.* **119** (2024) 233 https://doi.org/10.1134/S0021364023603755